**Beam Physics Note**
TRI-BN-23-30
December 15, 2023

# IMS to Polarizer Beam Transport

Olivier Shelbaya, Emma Ghelfi, Giordano Kogler Anele,
Rick Baartman

TRIUMF

**Abstract:** The ISAC Mass Separator network of beamlines is added to the `/acc` database, enabling realtime TRANSOPTR-supported tuning using model coupled accelerator tuning. Baartman's original TRANSOPTR simulations and design tune are used to simulate IMS to polarizer beam transport.

4004 Wesbrook Mall, Vancouver, B.C. Canada V6T 2A3 · Tel: 604 222-1047 · www.triumf.ca

# Contents

# 1 Introduction

This document records the implementation of the TRANSOPTR model of the ISAC mass separator (IMS) section in the acc repository, enabling automated generation of simulations and use of MCAT[1] for the ISAC Mass Separator beamlines. Note: All presented dimensions in this report are metric.

## 1.1 Sequence ims_mb1

The sequence includes the pre-separator dipole magnet, whose simulation parameters are shown in Table 1. Table 2 shows the sequence, including starting at ITW:IV5 centerpoint and terminating at IMS:IV0 centerpoint. A diagram including pre-separator is shown in Figure 1.

| Parameter | Value |
|---|---|
| $\theta$ [deg] | -60.0 |
| Entrance edge [deg] | 15.0 |
| Exit edge [deg] | 0.0 |
| field index | 0.0 |
| k1 | 0.200 |
| k2 | 0.0 |
| Vac. Chamb. Gap [cm] | 7.0 |

Table 1: Parameters supplied to TRANSOPTR for ISAC pre-separator magnet.

| sequence ims_mb1 | | | |
|---|---|---|---|
| Source | | ISK4214D-R99 | |
| Drawing | | Figure 1 | |
| Element Name | Element Type | Position S[mm] | Length L[mm] |
| start sequence | marker | 0.0 | 0.0 |
| IMS:MB1 | y-dipole (mb) | 699.41 | 547.69 |
| end sequence | marker | 1320.85 | 0.0 |

Table 2: Sequence ims_mb1, the pre-separator downstream of the ISAC targets. All element positions are referenced to the drawing listed in the table.

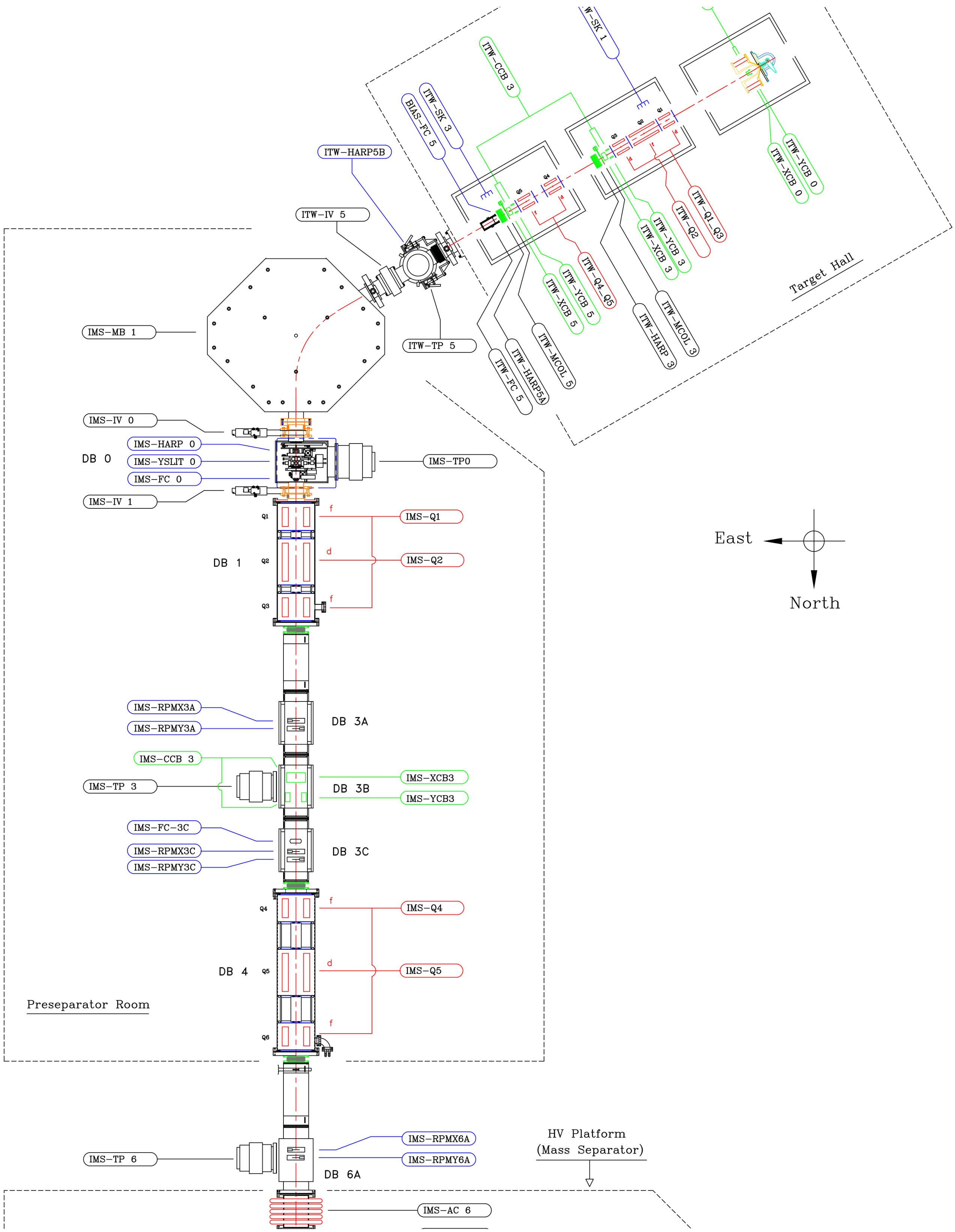


Figure 1: Sketch drawing `ISK4214D-R99.dwg`, showing ITW source, exit module, preseparator (IMS:MB0), and the first IMS straight section, up to the HV cage.

## 1.2 Sequence `ims_db0.xml`

This sequence, listed in Table 3, starts at IMS:IV0 centerpoint and terminates at the start of the IMS high voltage cage, prior to AC6. This sequence was taken from design `TRANSOPTR` files supplied by R. Baartman.

| sequence `ims_db0` | | | |
|---|---|---|---|
| Source | | Baartman `sy.f` | |
| Drawing | | Figure 1 | |
| Element Name | Type | Position $s$ [mm] | Length $L$ [mm] |
| start sequence | `marker` | 0.0 | 0.0 |
| Fringe Integrals | `fringeQ` | 0.0 | 0.0 |
| IMS:YSLIT0 | `slit` | 196.32 | 0.0 |
| IMS:FC0† | `fc` | 304.28 | 0.0 |
| IMS:Q1 | `EQuad` | 534.90 | 142.494 |
| IMS:Q2 | `EQuad` | 836.12 | 269.494 |
| IMS:Q3 | `EQuad` | 1137.34 | 142.494 |
| IMS:RPMX3A | `rpm` | 1936.68 | 0.0 |
| IMS:RPMY3A† | `rpm` | 1937.00 | 0.0 |
| IMS:XCB3† | `ecb` | 2331.39 | 0.0 |
| IMS:YCB3† | `ecb` | 2431.47 | 0.0 |
| IMS:FC3† | `fc` | 2600.01 | 0.0 |
| IMS:RPMX3C | `rpm` | 2787.83 | 0.0 |
| IMS:RPMY3C† | `rpm` | 2788.00 | 0.0 |
| IMS:Q4 | `EQuad` | 3150.04 | 142.494 |
| IMS:Q5 | `EQuad` | 3578.28 | 269.494 |
| IMS:Q6 | `EQuad` | 4006.52 | 142.494 |
| IMS:RPMY6A | `rpm` | 4819.32 | 0.0 |
| IMS:RPMX6A | `rpm` | 4844.72 | 0.0 |
| end sequence | `marker` | 5082.87 | 0.0 |

Table 3: Sequence `ims_db0`, the first optics section in the mass separator room, prior to the high voltage cage. † indicates approximate placement. A call to `fringeQ` using Wollnik integrals[2] using $(I_1, I_2, I_3, I_4)$ = (0.092,0.000,0.031,-0.238) is used at the start of the above sequence.

## 1.3 Sequence `ims_db6.xml`

This sequence, listed in Table 4, includes the high voltage cage and mass separator magnet, shown in Figure 2, using parameters from Table 5. Dimensions obtained from Baartman's design `sy.f` files. Envelopes and distributions from yslit0, through the mass separator up to IMS:FC14 are shown in Fig. 7 and 8.

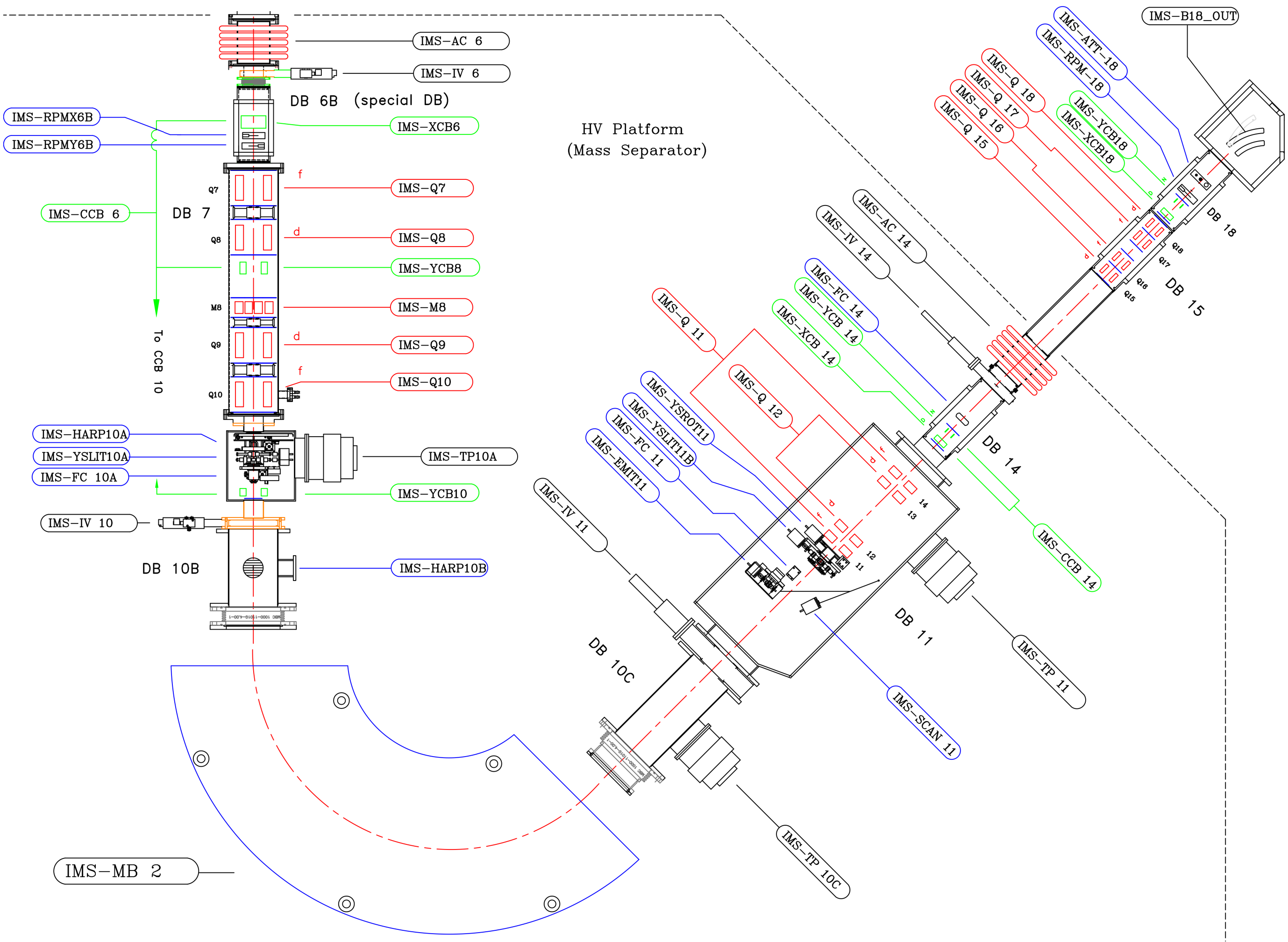


Figure 2: Sketch drawing `ISK4214D-R99.dwg`, including IMS HV cage, mass separator magnet and emittance rig. The outer bounds of the HV cage is represented by a dotted line.

sequence `ims_db6`

| Element Name | Element Type | Position $s$ [mm] | Length $L$ [mm] |
|---|---|---|---|
| Source | | Baartman `sy.f` | |
| Design Drawing | | Figure 2 | |
| start sequence | `marker` | 0.0 | 0.0 |
| Fringe Integrals | `fringeQ` | 0.0 | 0.0 |
| IMS:XCB6† | `ecb` | 525.39 | 0.0 |
| IMS:RPMX6B | `rpm` | 559.41 | 0.0 |
| IMS:RPMY6B | `rpm` | 622.91 | 0.0 |
| IMS:Q7 | `EQuad` | 835.26 | 142.494 |
| IMS:Q8 | `EQuad` | 1086.97 | 142.494 |
| IMS:YCB8† | `ecb` | 1270.62 | 0.0 |
| IMS:M8 | `marker` | 1445.11 | 0.0 |
| IMS:Q9 | `EQuad` | 1638.41 | 142.494 |
| IMS:Q10 | `EQuad` | 1890.12 | 142.494 |
| IMS:YSLIT10A | `slit` | 2242.16 | var. width |
| IMS:FC10A† | `fc` | 2351.00 | 0.0 |
| IMS:YCB10† | `ecb` | 2414.97 | 0.0 |
| IMS:HARP10B | `harp` | 2800.96 | 0.0 |
| IMS:MB2 | `y-dipole (mb)` | 4471.82 | 2356.194 |
| IMS:EMIT11† | `marker` | 7026.46 | 0.0 |
| IMS:FC11 | `fc` | 7159.00 | 0.0 |
| IMS:YSLIT11B | `slit` | 7267.91 | var. width |
| Fringe Integrals | `fringeQ` | 7300.00 | 0.0 |
| IMS:Q11 | `EQuad` | 7431.74 | 60.96 |
| IMS:Q12 | `EQuad` | 7507.94 | 66.04 |
| IMS:Q12 | `EQuad` | 7871.15 | 66.04 |
| IMS:Q11 | `EQuad` | 7949.89 | 66.04 |
| IMS:XCB14† | `ecb` | 8134.59 | 0.0 |
| IMS:YCB14† | `ecb` | 8197.19 | 0.0 |
| IMS:FC14† | `fc` | 8292.80 | 0.0 |
| IMS:RPM14† | `rpm` | 8392.80 | 0.0 |
| end sequence | `marker` | 8826.82 | 0.0 |

Table 4: Sequence `ims_db6`, the high voltage platform, including mass separator magnet and emittance rig. † indicates approximate placement. The `fringeQ` uses $(I_1, I_2, I_3, I_4)$ = (0.092,0.000,0.031,-0.238), while the second uses `fringeQ` call use $(I_1, I_2, I_3, I_4)$ = (0.087,0.005,0.033,-0.234).

| Parameter | Value |
|---|---|
| $\theta$ [deg] | 135.0 |
| Entrance edge [deg] | 0.0 |
| Exit edge [deg] | 0.0 |
| field index | 0.506 |
| k1 | 0.260 |
| k2 | 0.0 |
| Vac. Chamb. Gap [cm] | 10.0 |

Table 5: Parameters supplied to TRANSOPTR for ISAC mass separator magnet (IMS:MB2).

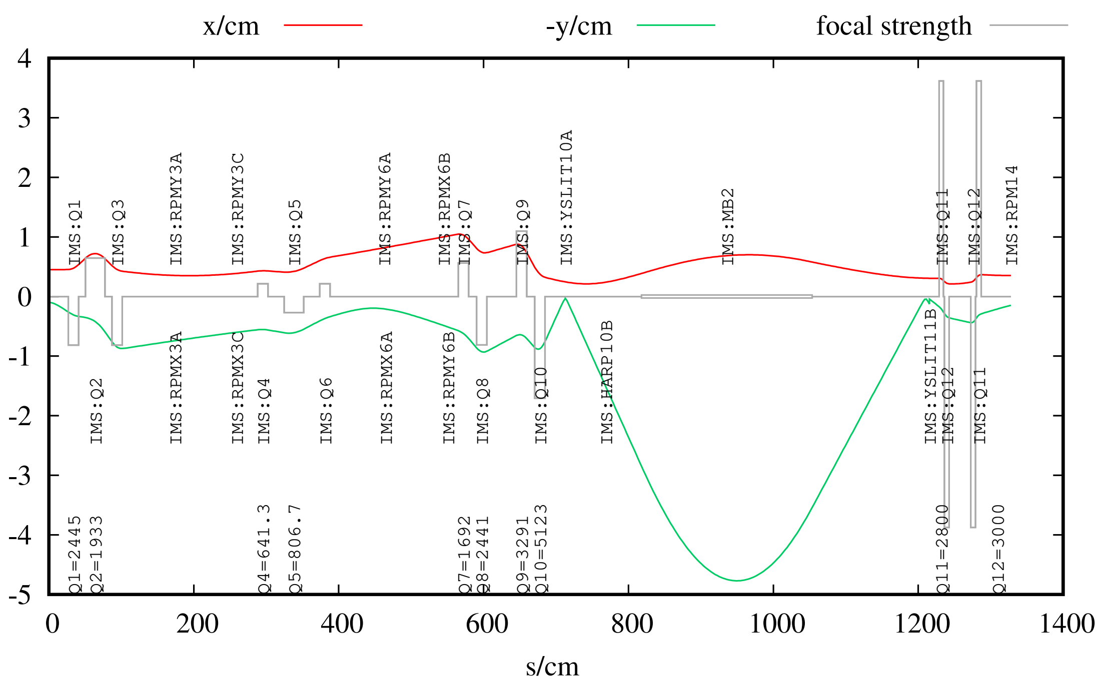


Figure 3: TRANSOPTR envelopes of an $A/q = 200$ beam at kinetic energy 60 keV, from yslit0 until the exit of the mass separator, encompassing sequences from Tables 3 and 4. Quadrupole voltages shown at the bottom of the plot.

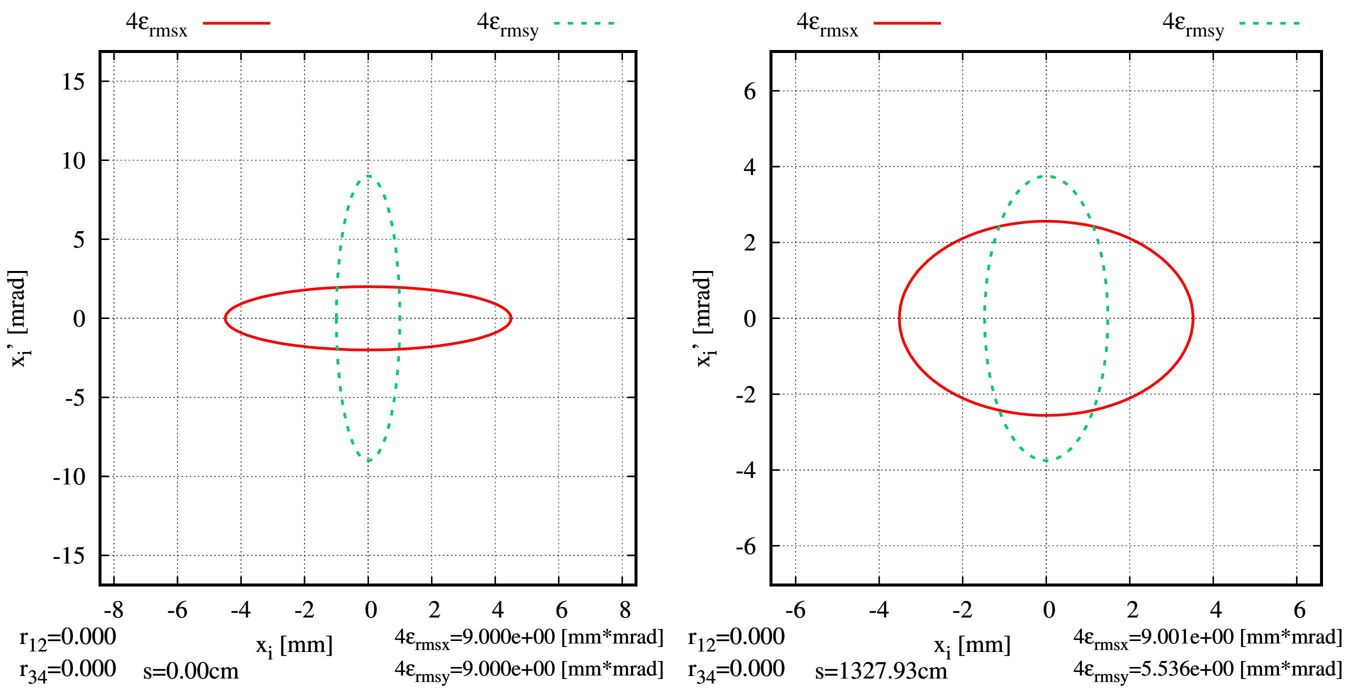


Figure 4: **Left:** transverse beam distributions at $s = 0$ (IMS:YSLIT0) and **right:** output transverse distributions at the end of the simulation (IMS:RPM14) shown in Figure 7.

## 1.4 Sequence `ims_db15.xml`

The sequence is shown in Figure 5 and includes spherical electrostatic bender IMS:B18 with parameters listed in listed in Table 6, is shown in Table. 7. It starts after the HV cage and terminates immediately upstream of bender IMS:B23.

| Parameter | Value |
|---|---|
| $\theta$ [deg] | -45.00 |
| k1 | 0.212 |
| cee | 1.00 |
| Electrode Gap [cm] | 3.810 |

Table 6: Parameters used for spherical bender IMS:B18; `cee` is the ratio of bend radius to orthogonal radius.

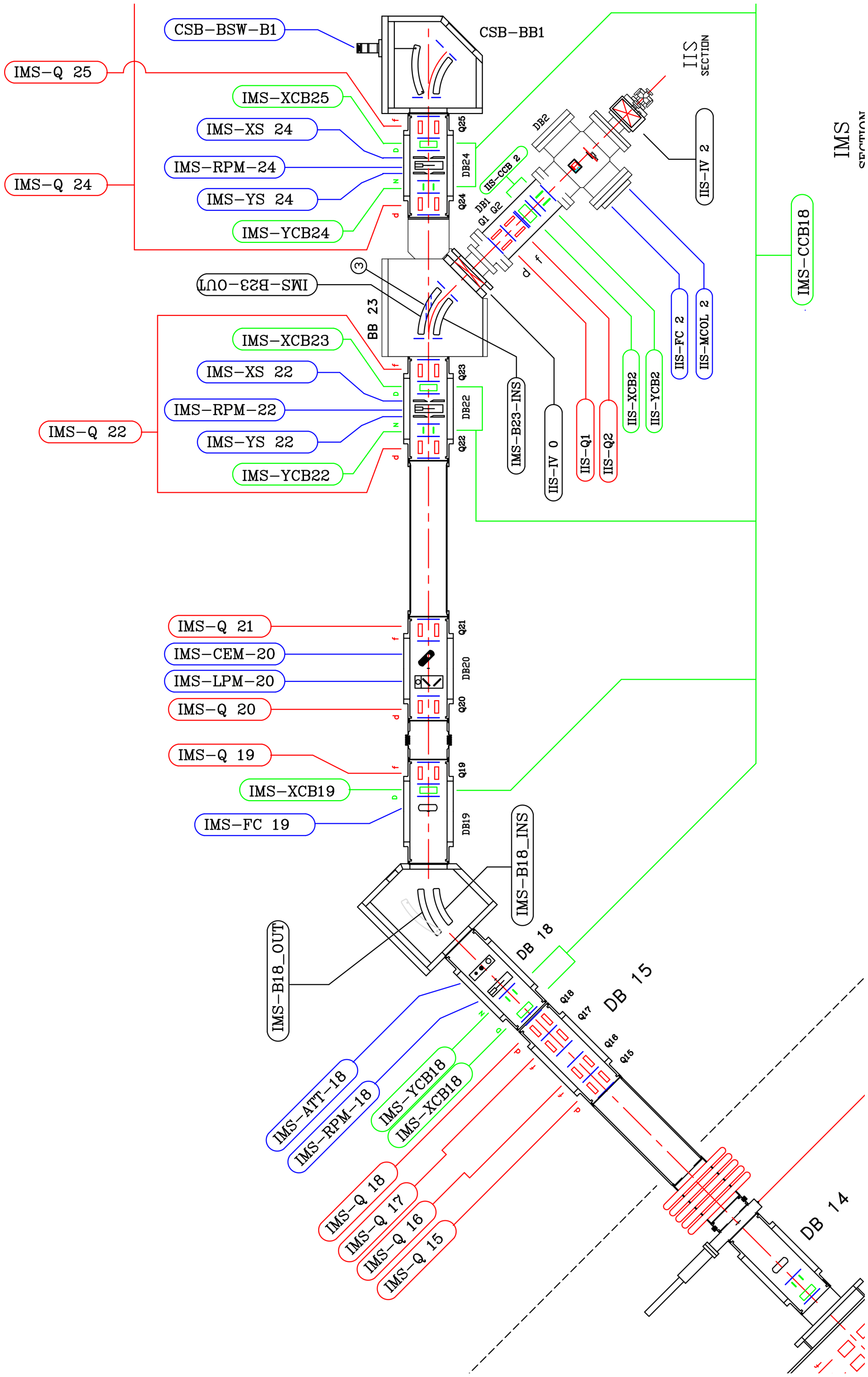


Figure 5: Sketch drawing ISK4214D-R99.dwg, showing IMS line out of the HV cage, featuring both spherical benders IMS:B23 (IIS) and CSB:B1 (CSB). The outer bounds of the HV cage is represented by a dotted line.

| sequence ims_db15 | | | |
|---|---|---|---|
| Source | | Baartman sy.f | |
| Design Drawing | | Figure 5 | |
| Element Name | Element Type | Position $s$ [mm] | Length $L$ [mm] |
| start sequence | marker | 0.0 | 0.0 |
| IMS:Q15 | EQuad | 427.36 | 61.14 |
| IMS:Q16 | EQuad | 516.25 | 61.14 |
| IMS:Q17 | EQuad | 668.62 | 61.14 |
| IMS:Q18 | EQuad | 757.51 | 61.14 |
| IMS:XCB18† | ecb | 944.83 | 0.0 |
| IMS:YCB18† | ecb | 1025.94 | 0.0 |
| IMS:RPM18† | rpm | 1095.55 | 0.0 |
| IMS:ATT18† | marker | 1190.64 | 0.0 |
| IMS:B18 | yeb | 1418.50 | 199.49 |
| IMS:FC19† | fc | 1860.91 | 0.0 |
| IMS:XCB19† | ecb | 1945.15 | 0.0 |
| IMS:Q19 | EQuad | 1982.28 | 61.14 |
| IMS:Q20 | EQuad | 2247.38 | 61.14 |
| IMS:LPM20† | marker | 2387.92 | 0.0 |
| IMS:CEM20† | marker | 2494.76 | 0.0 |
| IMS:Q21 | EQuad | 2561.48 | 61.14 |
| IMS:Q22 | EQuad | 3316.44 | 61.14 |
| IMS:YCB22† | ecb | 3417.98 | 0.0 |
| IMS:YSLIT22† | slit | 3471.72 | 0.0 |
| IMS:RPM22† | rpm | 3505.71 | 0.0 |
| IMS:XSLIT22† | slit | 3535.22 | 0.0 |
| IMS:XCB23† | ecb | 3592.23 | 0.0 |
| IMS:Q23 | EQuad | 3630.49 | 61.14 |
| end sequence | marker | 3791.51 | 0.0 |

Table 7: Sequence ims_db15, the optics following the post-MB2 doublet (Q11/12). † indicates approximate placement. All quadrupoles in this sequence use Wollnik integrals $(I_1, I_2, I_3, I_4)$ = (0.087,0.005,0.033,-0.234).

## 1.5 Sequence `ims_db24.xml`

This sequence is shown in Figure 5 and has dimensions listed in 8. It starts at intersection between curved and straight reference trajectories at IMS:B23, continuing straight (B23 open, unpowered) to the branch point between straight and curved reference trajectories at CSB:B1, which terminates the sequence. In the present sequence, IMS:B23 is only represented as a marker.

| sequence `ims_db24` | | | |
|---|---|---|---|
| Source | | Baartman `sy.f` | |
| Design Drawing | | Figure 5 | |
| Element Name | Element Type | Position $s$ [mm] | Length $L$ [mm] |
| start sequence | `marker` | 0.0 | 0.0 |
| IMS:B23 | `marker` | 0.0 | 0.0 |
| IMS:Q24 | `EQuad` | 519.98 | 61.14 |
| IMS:YCB24 | `ecb` | 621.88 | 0.0 |
| IMS:YSLIT24$^\dagger$ | `slit` | 675.52 | var. width |
| IMS:XCB25 | `ecb` | 796.12 | 0.0 |
| IMS:RPM24$^\dagger$ | `rpm` | 710.00 | 0.0 |
| IMS:XSLIT24$^\dagger$ | `slit` | 739.02 | var. width |
| IMS:Q25 | `EQuad` | 834.13 | 61.14 |
| end sequence | `marker` | 964.27 | 0.0 |

Table 8: Sequence `ims_db24`, the short straight section between spherical bend electrodes IMS:B23 and CSB:B1. $^\dagger$ indicates approximate placement. All quadrupoles in this sequence use Wollnik integrals $(I_1, I_2, I_3, I_4)$ = (0.087,0.005,0.033,-0.234).

## 1.6 Sequence `ims_db26.xml`

The sequence starts at the intersection between IMS and CSB beamlines and terminates after IMS:Q37 and is shown in Figure 6 and listed in Table 9. All spherical benders parameters as shown in Table 6.

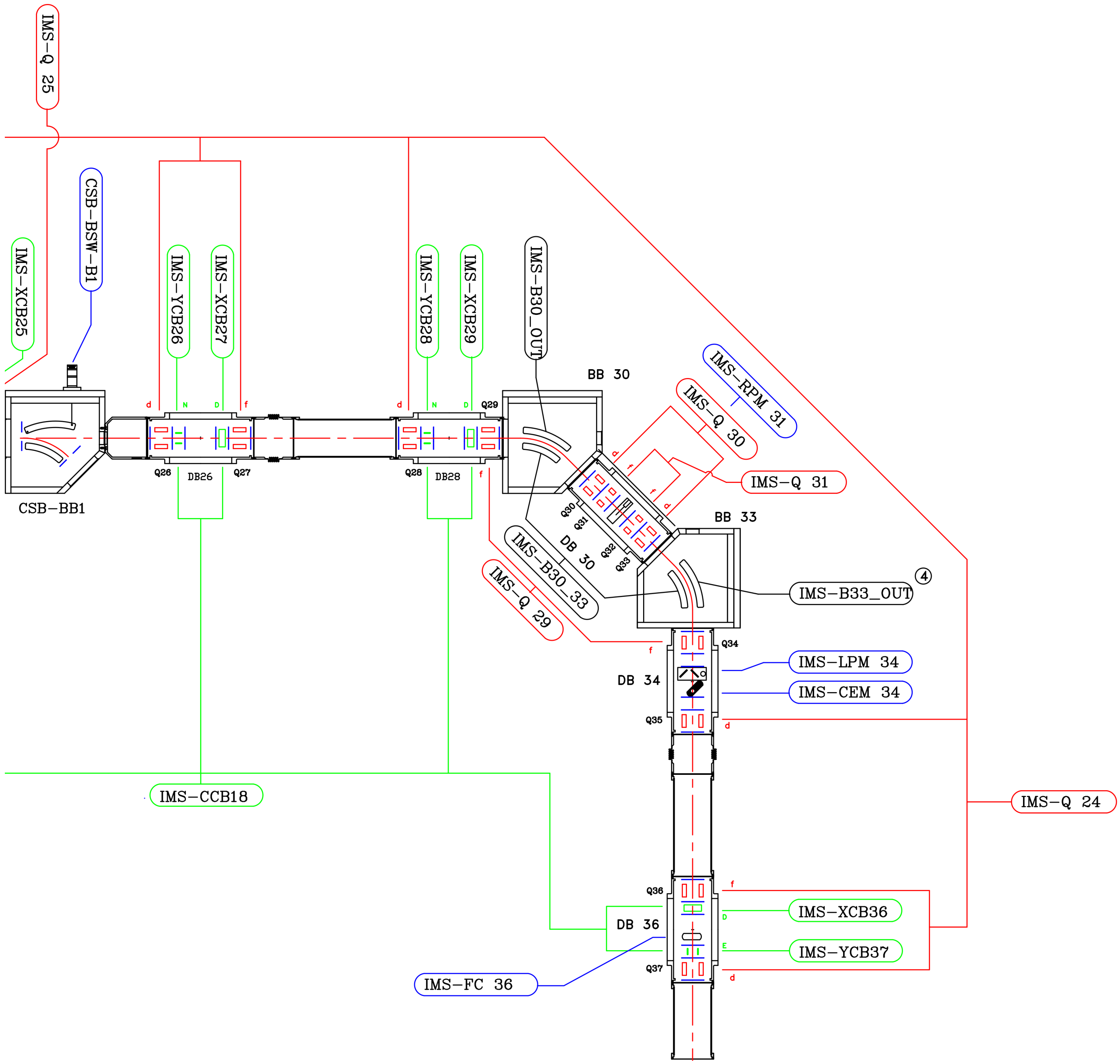


Figure 6: Sketch drawing `ISK4214D-R99.dwg`, showing IMS following CSB:B1, up to IMS:Q37.

sequence `ims_db26`

| Source | | Baartman `sy.f` | |
|---|---|---|---|
| Design Drawing | | Figure 6 | |
| Element Name | Element Type | Position $s$ [mm] | Length $L$ [mm] |
| start sequence | `marker` | 0.0 | 0.0 |
| CSB:B1 | `marker` | 0.0 | 0.0 |
| IMS:Q26 | `EQuad` | 551.44 | 61.14 |
| IMS:YCB26$^{\dagger}$ | `ecb` | 621.30 | 0.0 |
| IMS:XCB27$^{\dagger}$ | `ecb` | 795.55 | 0.0 |
| IMS:Q27 | `EQuad` | 865.41 | 61.14 |
| IMS:YCB28$^{\dagger}$ | `ecb` | 1615.85 | 0.0 |
| IMS:XCB29$^{\dagger}$ | `ecb` | 1790.09 | 0.0 |
| IMS:Q28 | `EQuad` | 1545.99 | 61.14 |
| IMS:Q29 | `EQuad` | 1859.96 | 61.14 |
| IMS:B30 | `yeb` | 2089.33 | 199.49 |
| IMS:Q30 | `EQuad` | 2350.39 | 48.44 |
| IMS:Q31 | `EQuad` | 2420.24 | 35.74 |
| IMS:RPM31$^{\dagger}$ | `rpm` | 2496.08 | 0.0 |
| IMS:Q32 | `EQuad` | 2568.07 | 35.74 |
| IMS:Q33 | `EQuad` | 2637.92 | 48.44 |
| IMS:B33 | `yeb` | 2901.32 | 199.49 |
| IMS:Q34 | `EQuad` | 3129.15 | 61.14 |
| IMS:LPM34$^{\dagger}$ | `lpm` | 3251.13 | 0.0 |
| IMS:CEM34$^{\dagger}$ | `cem` | 3326.97 | 0.0 |
| IMS:FC34$^{\dagger}$ | `fc` | 3326.97 | 0.0 |
| IMS:Q35 | `EQuad` | 3443.10 | 61.14 |
| IMS:Q36 | `EQuad` | 4123.56 | 61.14 |
| IMS:XCB36$^{\dagger}$ | `ecb` | 4196.57 | 0.0 |
| IMS:YCB37$^{\dagger}$ | `ecb` | 4370.82 | 0.0 |
| IMS:Q37 | `EQuad` | 4437.48 | 61.14 |
| end sequence | `marker` | 4494.66 | 0.0 |

Table 9: Sequence `ims_db26`, the section following the open CSB:B1, which terminates beyond IMS:Q37. $^{\dagger}$ indicates approximate placement. All quadrupoles in this sequence use Wollnik integrals $(I_1, I_2, I_3, I_4)$ = (0.087,0.005,0.033,-0.234).

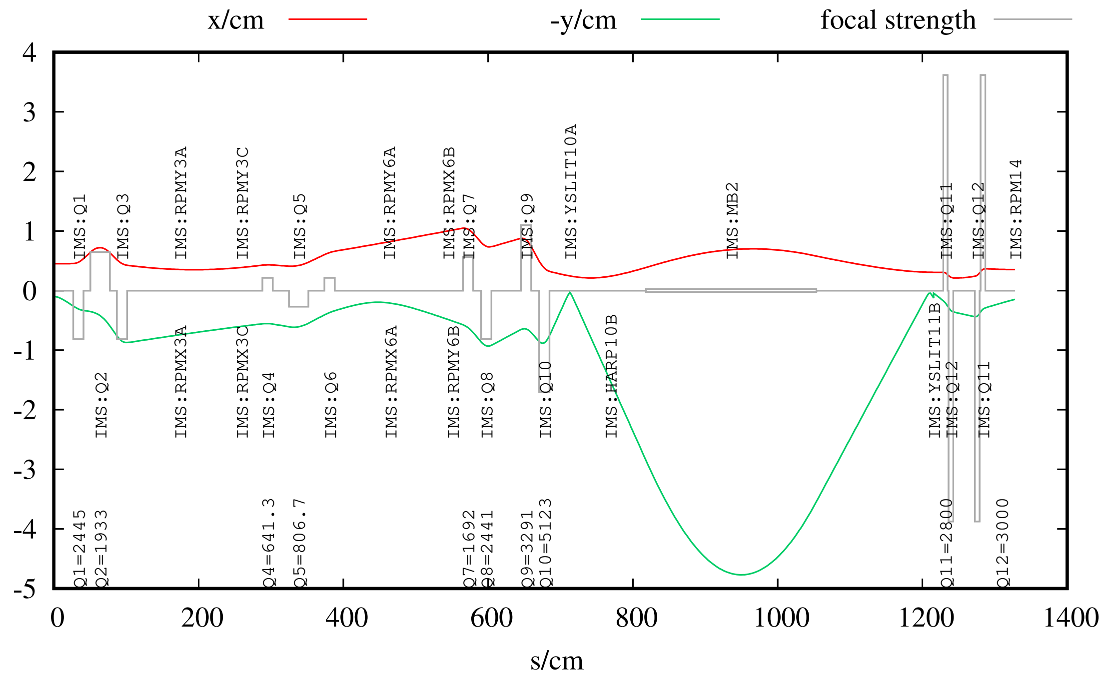


Figure 7: TRANSOPTR envelopes of an $A/q = 200$ beam at kinetic energy 60 keV, from yslit0 until the exit of the mass separator, encompassing sequences from Tables 3 and 4. Quadrupole voltages shown at the bottom of the plot.

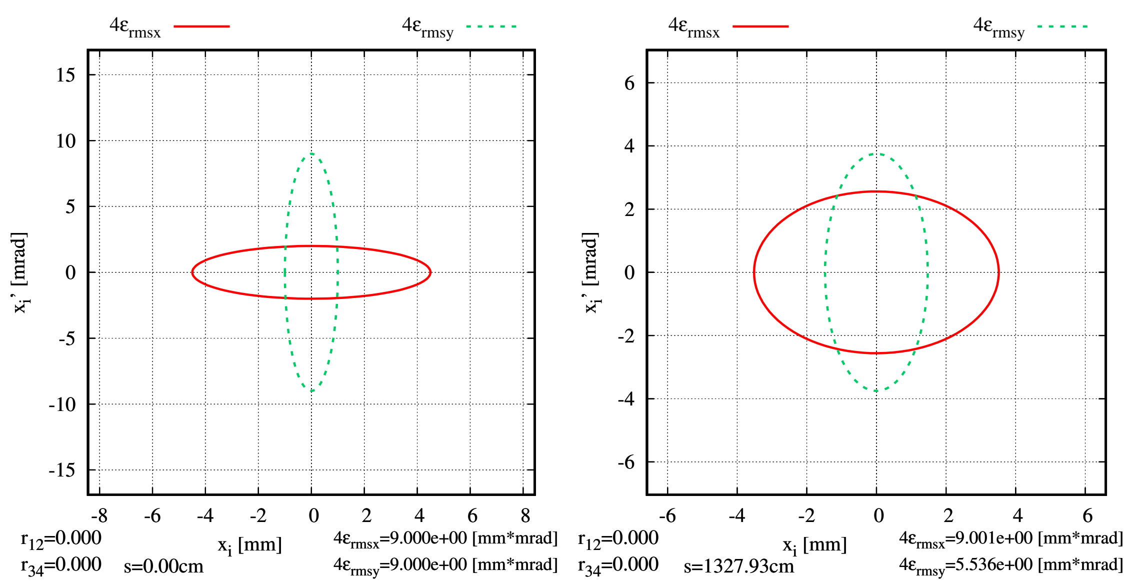


Figure 8: **Left:** transverse beam distributions at $s = 0$ (IMS:YSLIT0) and **right:** output transverse distributions at the end of the simulation (IMS:RPM14) shown in Figure 7.

## 1.7 Sequence `ilt_db1.xml`

This sequence, shown in Table 10, starts at the end of the IMS section with quadrupoles ILT:Q1 and Q2 leading into the vertical bend section leading to the ILT beamline, with a sketch representation in Figure 9.

sequence `ilt_db1`

| Source | | Baartman `sy.f` | |
|---|---|---|---|
| Design Drawing | | Figure 9 | |
| Element Name | Element Type | Position $s$ [mm] | Length $L$ [mm] |
| start sequence | `marker` | 0.0 | 0.0 |
| ILT:Q1 | `EQuad` | 589.36 | 60.96 |
| ILT:XCB1† | `ecb` | 690.83 | 0.0 |
| ILT:RPM1† | `marker` | 778.13 | 0.0 |
| ILT:YCB2† | `ecb` | 865.08 | 0.0 |
| ILT:Q2 | `EQuad` | 903.47 | 60.96 |
| ILT:VB3 | `eb` | 1131.09 | 199.49 |
| ILT:Q3† | `EQuad` | 1394.67 | 48.26 |
| ILT:Q4 | `EQuad` | 1464.50 | 35.56 |
| ILT:RPM4† | `marker` | 1565.97 | 0.0 |
| ILT:Q5 | `EQuad` | 1612.39 | 35.56 |
| ILT:Q6 | `EQuad` | 1682.19 | 48.26 |
| ILT:VB6 | `eb` | 1925.75 | 159.47 |
| ILT:YCB7† | `ecb` | 2176.54 | 0.0 |
| ILT:XCB7† | `deflx` | 2239.89 | 50.65 |
| end sequence | `marker` | 2265.20 | 0.0 |

Table 10: Sequence `ilt_db1`, the optics leading into the vertical section. † indicates approximate placement. All quadrupoles in this sequence use Wollnik integrals $(I_1, I_2, I_3, I_4)$ = (0.087,0.005,0.033,-0.234). ILT:VB3 is a 45° spherical, while ILT:VB6 is a $\theta$=36° spherical bender. Both devices have k1, *cee* and Gap identical to Table 6. ILT:XCB7 is a 9° degree x-deflector.

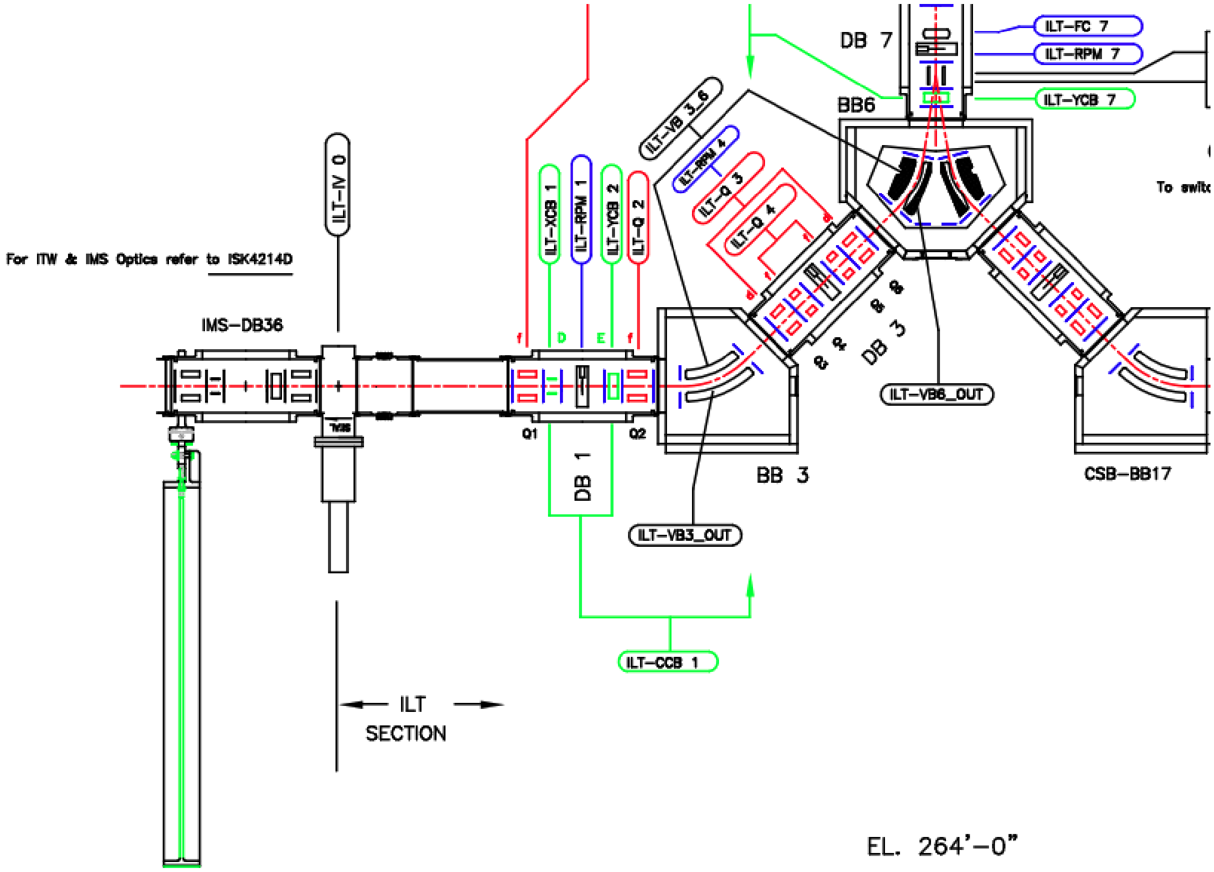


Figure 9: Sketch drawing `ISK4210D-rev4.dwg`, showing ILT section following end of the IMS section

## 1.8 Sequence `ilt_db7.xml`

The sequence, shown in Figure 10, is listed in Table 11 and contains the first part of the ILT vertical section, linking IMS and ISAC experiments. This sequence ends before the movable spherical bender that allows beam to be sent to TRINAT (ILY) or to continue upward in the ILT line, towards yield station (ILY) and ISAC-I experimental hall floor.

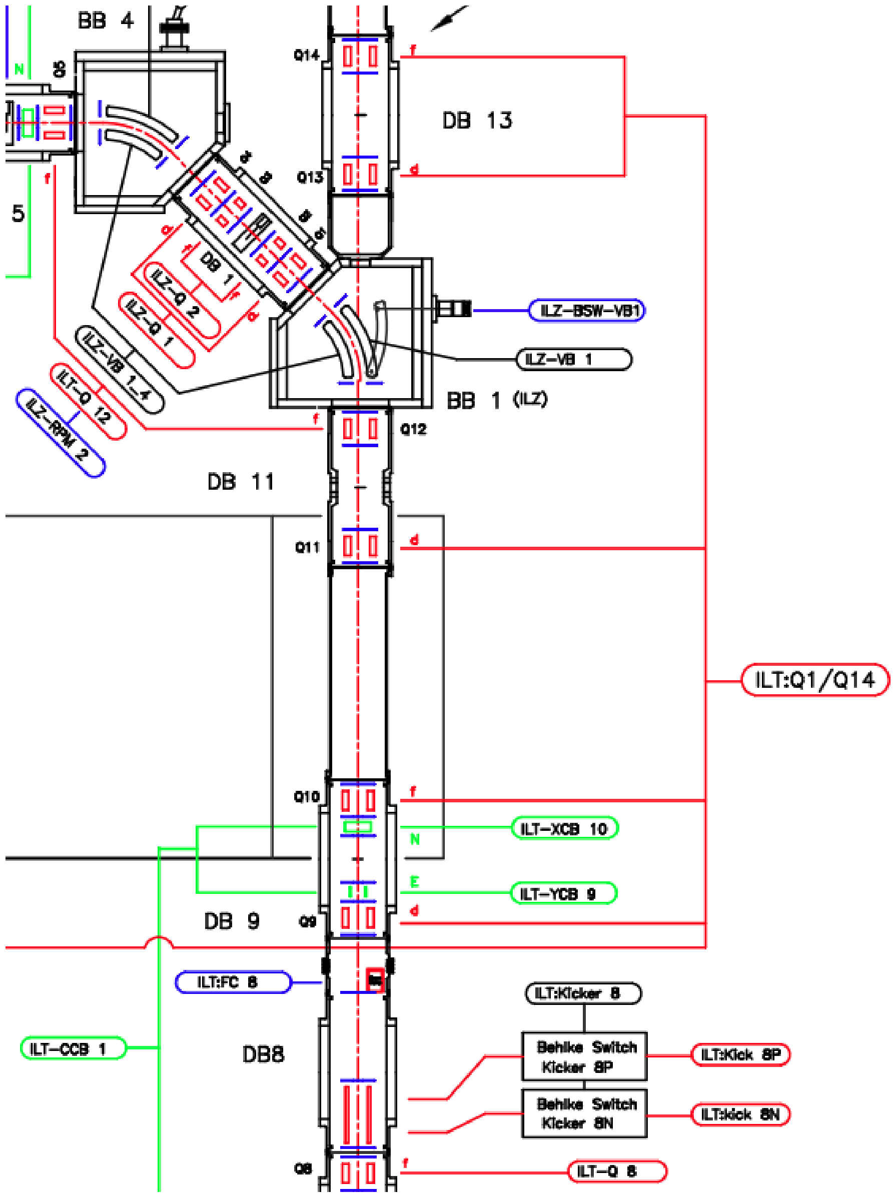


Figure 10: Sketch drawing `ISK4210-rev4.dwg`, showing first vertical segment of the ILT line, with this particular image terminating after the movable bend electrode to the TRINAT (ILZ) experiment. Note interconnection of quadrupoles ILT:Q9,10,11,13 and 14 to `EPICS` variable `ILT:Q1`.

| sequence `ilt_db7` | | | |
|---|---|---|---|
| Source | | Baartman `sy.f` | |
| Design Drawing | | Figure 9 | |
| Element Name | Element Type | Position $s$ [mm] | Length $L$ [mm] |
| start sequence | `marker` | 0.0 | 0.0 |
| ILT:RPM7† | `marker` | 8.68 | 0.0 |
| IMS:FC7† | `fc` | 91.01 | 0.0 |
| ILT:Q8 | `EQuad` | 247.27 | 61.14 |
| ILT:KICK8† | `marker` | 428.24 | 0.0 |
| ILT:Q9 | `EQuad` | 928.05 | 61.14 |
| ILT:YCB9† | `ecb` | 987.55 | 0.0 |
| ILT:XCB10† | `ecb` | 1160.78 | 0.0 |
| ILT:Q10 | `EQuad` | 1242.01 | 61.14 |
| ILT:Q11 | `EQuad` | 1922.41 | 61.14 |
| ILT:Q12 | `EQuad` | 2236.37 | 61.14 |
| end sequence | `marker` | 2270.14 | 0.0 |

Table 11: Sequence `ilt_db7`, the optics ij the vertical section. † indicates approximate placement. All quadrupoles in this sequence use Wollnik integrals $(I_1, I_2, I_3, I_4)$ = (0.087,0.004,0.031,-0.232).

## 1.9 Sequence `ilt_db13.xml`

This sequence is shown in Figure 11 and the dimensions are shown in Table 12. Transport through this section assumes the spherical bender ILZ:VB1 to TRINAT (ILY) is open/unpowered, and encompasses the second part of the ILT vertical section, terminating at the start of the bend section which leads to the ISAC experimental hall floor. This section is located in the ISAC-I B1 level, at the TRINAT level.

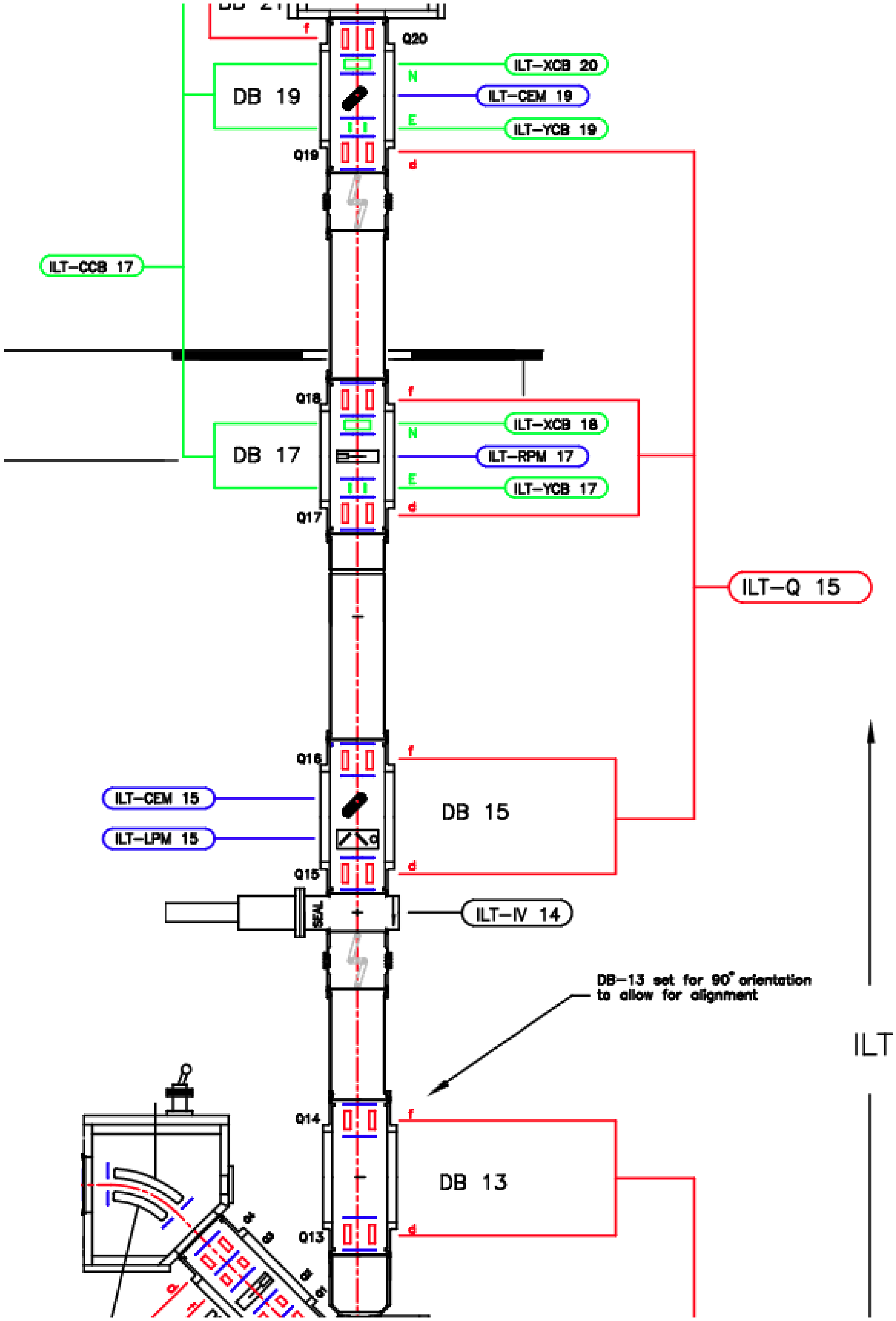


Figure 11: Sketch drawing `ISK4210D-rev4.dwg`, showing the second half of the vertical ILT section, linking IMS and ISAC experimental hall floor level.

sequence `ilt_db13`

| Source | | Baartman `sy.f` | |
|---|---|---|---|
| Design Drawing | | Figure 11 | |
| Element Name | Element Type | Position $s$ [mm] | Length $L$ [mm] |
| start sequence | `marker` | 0.0 | 0.0 |
| ILT:Q13 | `EQuad` | 646.99 | 61.14 |
| ILT:Q14 | `EQuad` | 960.94 | 61.14 |
| ILT:Q15 | `EQuad` | 1641.63 | 61.14 |
| ILT:LPM15$^\dagger$ | `marker` | 1724.80 | 0.0 |
| ILT:CEM15$^\dagger$ | `marker` | 1829.14 | 0.0 |
| ILT:Q16 | `EQuad` | 1955.58 | 61.14 |
| ILT:Q17 | `EQuad` | 2635.99 | 61.14 |
| ILT:YCB17$^\dagger$ | `ecb` | 2694.40 | 0.0 |
| ILT:RPM17$^\dagger$ | `marker` | 2781.38 | 0.0 |
| ILT:XCB18$^\dagger$ | `ecb` | 2867.62 | 0.0 |
| ILT:Q18 | `EQuad` | 2950.26 | 61.14 |
| ILT:Q19 | `EQuad` | 3630.74 | 61.14 |
| ILT:YCB19$^\dagger$ | `ecb` | 3689.71 | 0.0 |
| ILT:FC19$^\dagger$ | `fc` | 3778.00 | 0.0 |
| ILT:XCB20$^\dagger$ | `ecb` | 3863.96 | 0.0 |
| ILT:Q20 | `EQuad` | 3944.59 | 61.14 |
| end sequence | `marker` | 3978.43 | 0.0 |

Table 12: Sequence `ilt_db13`, the optics in the second half of the vertical section. $^\dagger$ indicates approximate placement. All quadrupoles in this sequence use Wollnik integrals $(I_1, I_2, I_3, I_4)$ = (0.087,0.004,0.031,-0.232).

## 1.10 Sequence `ilt_db21.xml`

This sequence consists of the achromatic bend section out of the vertical ILT section and into the ISAC experimental hall floor, with dimensions in Table 13 and a sketch drawing of the section shown in Figure 12.

| sequence `ilt_db21` | | | |
|---|---|---|---|
| Source | | Baartman `sy.f` | |
| Design Drawing | | Figure 12 | |
| Element Name | Element Type | Position $s$ [mm] | Length $L$ [mm] |
| start sequence | `marker` | 0.0 | 0.0 |
| ILT:VB21 | `yeb` | 203.15 | 199.49 |
| ILT:Q21 | `EQuad` | 464.98 | 46.23 |
| ILT:Q22 | `EQuad` | 534.82 | 33.53 |
| ILT:RPM22† | `marker` | 611.18 | 0.0 |
| ILT:Q23 | `EQuad` | 684.97 | 33.53 |
| ILT:Q24 | `EQuad` | 754.81 | 46.23 |
| ILT:VB24 | `yeb` | 1016.64 | 199.49 |
| ILT:Q25 | `EQuad` | 1245.09 | 58.93 |
| ILT:XCB25† | `ecb` | 1317.19 | 0.0 |
| ILT:FC25† | `fc` | 1370.45 | 0.0 |
| ILT:YCB26† | `ecb` | 1489.51 | 0.0 |
| ILT:Q26 | `EQuad` | 1559.01 | 58.93 |
| end sequence | `marker` | 1588.48 | 0.0 |

Table 13: Sequence `ilt_db21`, the optics in the second half of the vertical section. † indicates approximate placement. All quadrupoles in this sequence use Wollnik integrals $(I_1, I_2, I_3, I_4)$ = (0.087,0.004,0.031,-0.232).

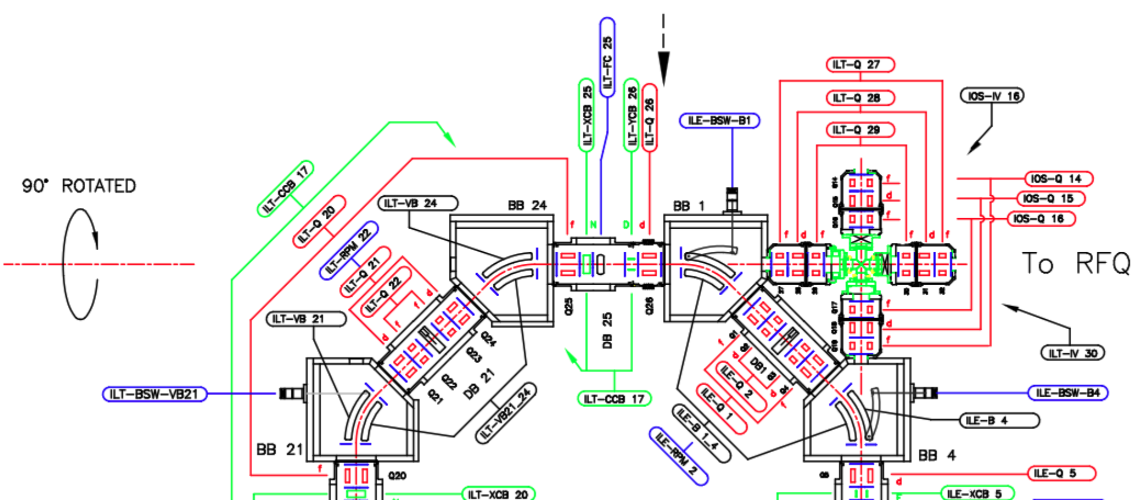


Figure 12: Sketch drawing `ISK4210D-rev4.dwg`, showing the final leg of the vertical ILT section, linking IMS and ISAC experimental hall floor level. Note 90° rotation of the reference frame.

## 1.11 Sequence `ile_db1.xml`

The section, shown in Figure 12 consists of an achromatic bend module in the horizontal plane in the ISAC experimental hall. It is located immediately downstream of the final ILT achromatic bend and allows beam to be transported toward the low energy section. Dimensions are shown in Table 14.

sequence `ile_db1`

| Source | | Baartman `sy.f` | |
|---|---|---|---|
| Design Drawing | | Figure 12 | |
| Element Name | Element Type | Position $s$ [mm] | Length $L$ [mm] |
| start sequence | `marker` | 0.0 | 0.0 |
| ILE:B1 | `eb` | 203.02 | 199.49 |
| ILE:Q1 | `EQuad` | 464.87 | 48.44 |
| ILE:Q2 | `EQuad` | 534.77 | 35.74 |
| ILE:RPM2† | `marker` | 611.37 | 0.0 |
| ILE:Q3 | `EQuad` | 684.87 | 35.74 |
| ILE:Q4 | `EQuad` | 754.67 | 48.44 |
| ILE:B4 | `eb` | 1016.51 | 199.49 |
| end sequence | `marker` | 1180.07 | 0.0 |

Table 14: Sequence `ile_db1`, the optics in the first achromatic bend section int he ISAC experimental hall, transporting beam toward the low energy experimental area. † indicates approximate placement. All quadrupoles in this sequence use Wollnik integrals $(I_1, I_2, I_3, I_4)$ = (0.087,0.004,0.031,-0.232).

## 1.12 Sequence `ile_db5.xml`

Sequence `ile_db5` starts at the end of the first ILE achromatic bend module and ends at the location of movable bender ILE1:B1, which allows transport to either the ILE1 line to GRIFFIN or transport to Francium/TITAN/Polarimeter and associated experiments. The dimensions are shown in Table 15 and the section shown in Figure 13.

sequence `ile_db5`

| Source | | Baartman `sy.f` | |
|---|---|---|---|
| Design Drawing | | Figure 13 | |
| Element Name | Element Type | Position $s$ [mm] | Length $L$ [mm] |
| start sequence | `marker` | 0.0 | 0.0 |
| ILE:Q5 | `EQuad` | 44.08 | 61.14 |
| ILE:XCB5 | `ecb` | 114.96 | 0.0 |
| ILE:RPM5† | `marker` | 175.53 | 0.0 |
| ILE:FC5† | `fc` | 231.97 | 0.0 |
| ILE:YCB6 | `ecb` | 289.76 | 0.0 |
| ILE:Q6 | `EQuad` | 358.10 | 61.14 |
| ILE:Q7 | `EQuad` | 571.80 | 61.14 |
| ILE:RPM7† | `marker` | 726.58 | 0.0 |
| ILE:Q8 | `EQuad` | 885.83 | 61.14 |
| ILE:Q9 | `EQuad` | 1100.73 | 61.14 |
| ILE:YCB9 | `ecb` | 1316.86 | 0.0 |
| ILE:XCB10 | `ecb` | 1347.82 | 0.0 |
| ILE:Q10 | `EQuad` | 1414.56 | 61.14 |
| end sequence | `marker` | 1543.36 | 0.0 |

Table 15: Sequence `ile_db5`, the optics in the straight section downstream of the first achromatic bend section in the ISAC experimental hall. † indicates approximate placement. All quadrupoles in this sequence use Wollnik integrals $(I_1, I_2, I_3, I_4)$ = (0.087,0.004,0.031,-0.232).

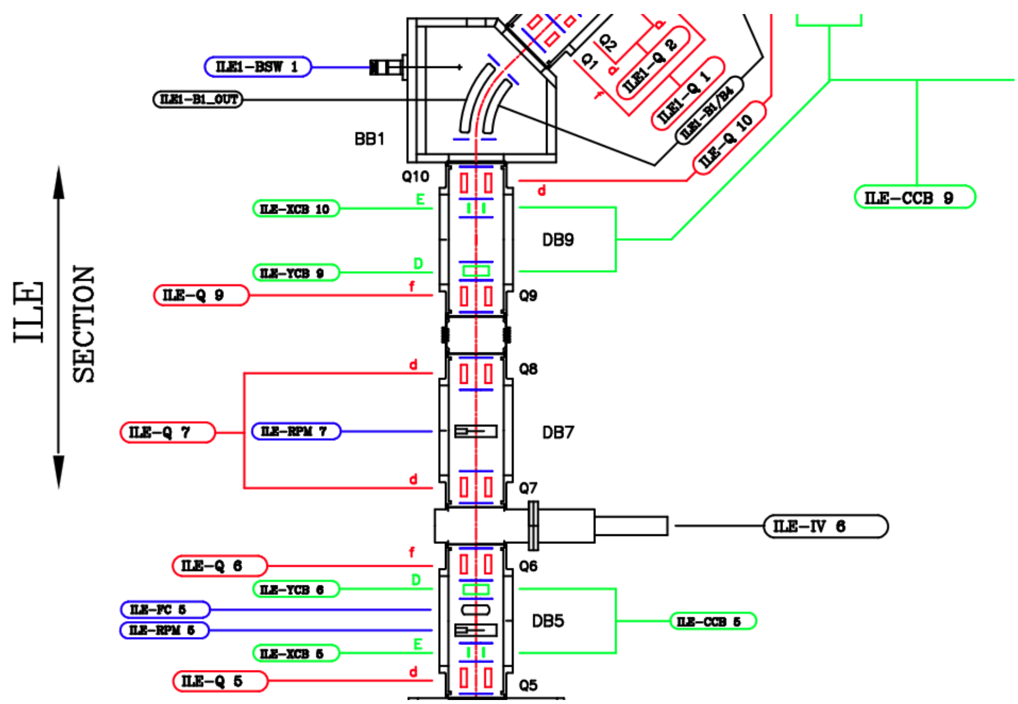


Figure 13: Sketch drawing `ISK4554D-rev2.dwg`, showing the ILE optics segment transporting beam to the switchyard between ILE1 and ILE2 experiments.

## 1.13 Sequence `ile_db11.xml`

Sequence `ile_db11` continues from the (open, unpowered) ILE1:B1, transporting beam toward Francium, TITAN and Polarizer. The sequence is shown in Figure 14 and recorded in Table 16.

sequence `ile_db11`

| Source | | Baartman `sy.f` | |
|---|---|---|---|
| Design Drawing | | Figure 14 | |
| Element Name | Element Type | Position $s$ [mm] | Length $L$ [mm] |
| start sequence | `marker` | 0.0 | 0.0 |
| ILE:Q11 | `EQuad/steer` | 531.08 | 61.14 |
| ILE:Q12 | `EQuad` | 845.05 | 61.14 |
| end sequence | `marker` | 973.27 | 0.0 |

Table 16: Sequence `ile_db11`, the optics in the straight section downstream of the movable bender ILE1:B1, which when open and unpowered, transports beam toward ILE2. $^\dagger$ indicates approximate placement. All quadrupoles in this sequence use Wollnik integrals $(I_1, I_2, I_3, I_4)$ = (0.085,0.004,0.031,-0.232).

## 1.14 Sequence `ile2_db1.xml`

Lower leg of the ILE2/ILE2T switchyard, recorded in Table 17, shown in Figure 14.

| sequence `ile2_db1` | | | |
|---|---|---|---|
| Source | | Baartman `sy.f` | |
| Design Drawing | | Figure 14 | |
| Element Name | Element Type | Position $s$ [mm] | Length $L$ [mm] |
| start sequence | `marker` | 0.0 | 0.0 |
| ILE2:B1 | `eb` | 99.75 | 199.49 |
| ILE2:Q1 | `EQuad` | 343.93 | 61.14 |
| ILE2:XCB1 | `ecb` | 418.78 | 0.0 |
| ILE2:FC1† | `fc` | 535.20 | 0.0 |
| ILE2:XCB2 | `ecb` | 555.94 | 0.0 |
| ILE2:Q2 | `EQuad` | 663.97 | 61.14 |
| end sequence | `marker` | 707.57 | 0.0 |

Table 17: Sequence `ile2_db1`, transporting beam toward Polarizer. ILE2:B1 parameters in Table 6. † indicates approximate placement. All quadrupoles in this sequence use Wollnik integrals $(I_1, I_2, I_3, I_4)$ = (0.085,0.004,0.031,-0.232).

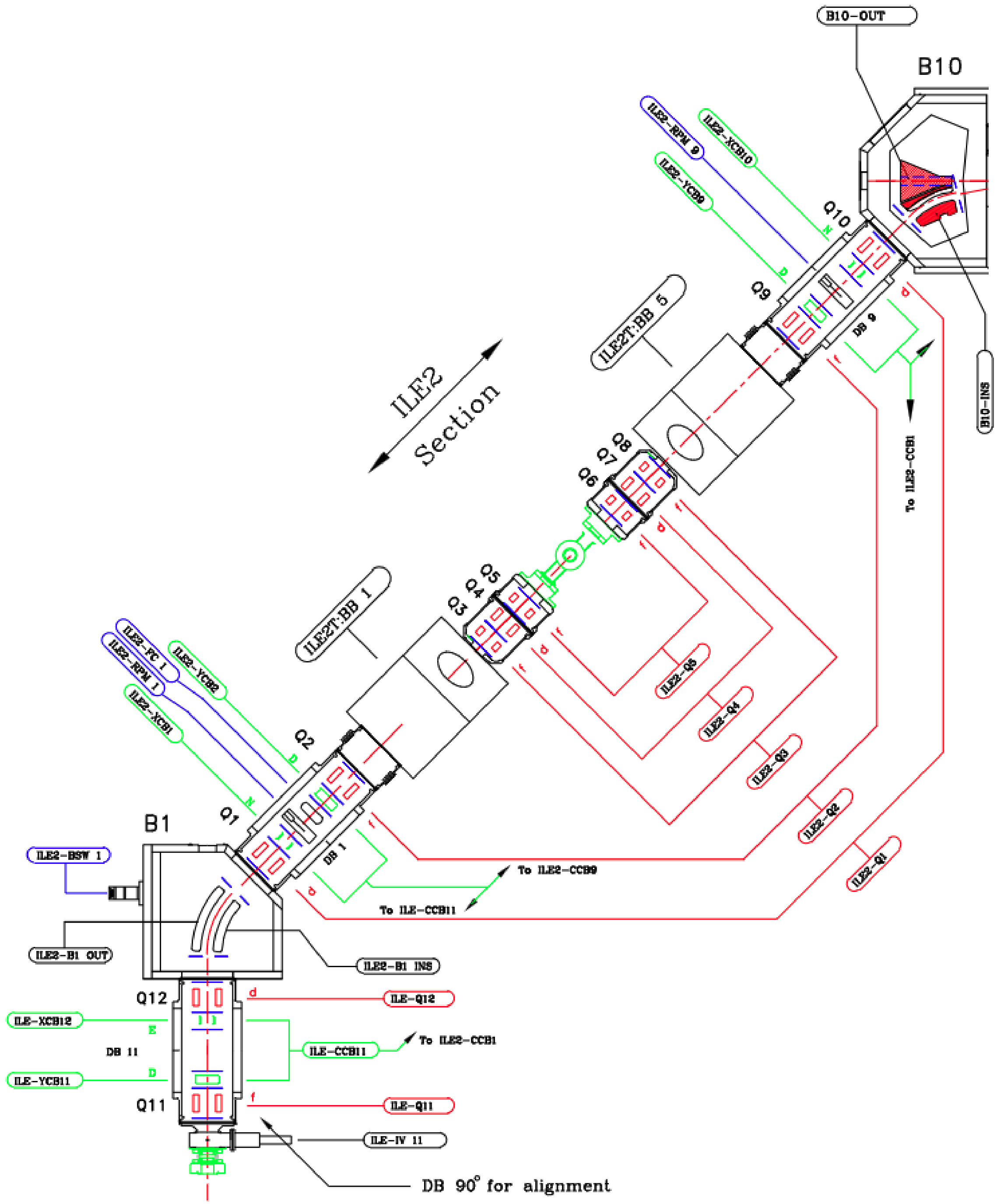


Figure 14: Sketch drawing `ISK4231D-rev11.dwg`, showing the ILE optics segment transporting beam to the switchyard between ILE2, ILE2T experiments.

## 1.15 Sequence `ile2_db3.xml`

This sequence is the central node of the ILE2/ILE2T switchyard section from Figure 14, and terminates at the branching point between the horizontal beamline and the 45° diagonal beamline leg coming down from the TITAN RFQ cooler-buncher. Dimensions are recorded in Table 18.

sequence `ile2_db3`

| Source | | Baartman `sy.f` | |
|---|---|---|---|
| Design Drawing | | Figure 14 | |
| Element Name | Element Type | Position $s$ [mm] | Length $L$ [mm] |
| start sequence | `marker` | 0.0 | 0.0 |
| ILE2:Q3 | `EQuad` | 563.61 | 25.40 |
| ILE2:Q4 | `EQuad` | 633.52 | 38.10 |
| ILE2:Q5 | `EQuad` | 703.44 | 25.40 |
| ILE2:Q6 | `EQuad` | 1121.10 | 25.40 |
| ILE2:Q7 | `EQuad` | 1191.08 | 38.10 |
| ILE2:Q8 | `EQuad` | 1260.90 | 25.40 |
| end sequence | `marker` | 1644.21.27 | 0.0 |

Table 18: Sequence `ile2_db3`, transporting beam toward Polarizer. $^{\dagger}$ indicates approximate placement. All quadrupoles in this sequence use Wollnik integrals $(I_1, I_2, I_3, I_4)$ = (0.085,0.004,0.031,-0.232).

## 1.16 Sequence `ile2_db9.xml`

The final sequence in this report is the polarizer line proper, with dimensions shown in Table 19, which starts at the top right hand side of Figure 14 (Q9) and continues in Figure 15.

| sequence `ile2_db9` | | | |
|---|---|---|---|
| Source | | Baartman `sy.f` | |
| Design Drawing | | Figure 14 | |
| Element Name | Element Type | Position $s$ [mm] | Length $L$ [mm] |
| start sequence | `marker` | 0.0 | 0.0 |
| ILE2:Q9 | `EQuad` | 223.98 | 61.14 |
| ILE2:YCB9 | `ecb` | 300.18 | 0.0 |
| ILE2:RPM9† | `marker` | 389.08 | 0.0 |
| ILE2:XCB10† | `ecb` | 465.28 | 0.0 |
| ILE2:Q10 | `EQuad` | 537.93 | 61.14 |
| ILE2:B10 | `eb` | 768.35 | 159.59 |
| ILE2:XCB11 | `deflx` | 1086.90 | 55.88 |
| ILE2:RPM11† | `marker` | 1158.78 | 0.0 |
| ILE2:FC11† | `fc` | 1209.58 | 0.0 |
| ILE2:YCB11 | `ecb` | 1265.34 | 0.0 |
| ILE2:Q11 | `EQuad` | 1327.71 | 61.14 |
| ILE2:Q12 | `EQuad` | 1859.88 | 61.14 |
| ILE2:Q13 | `EQuad` | 1946.75 | 61.14 |
| ILE2:Q14 | `EQuad` | 2098.26 | 61.14 |
| ILE2:Q15 | `EQuad` | 2187.67 | 61.14 |
| ILE2:XCB15† | `ecb` | 2275.17 | 0.0 |
| ILE2:YCB15† | `ecb` | 2326.63 | 0.0 |
| ILE2:RPM15† | `marker` | 2388.53 | 0.0 |
| ILE2:BIAS15† | `marker` | 2534.05 | 0.0 |
| ILE2:RBCELL† | `marker` | 2690.03 | 0.0 |
| ILE2:DEF15C† | `marker` | 3481.16 | 0.0 |
| ILE2:FC15† | `fc` | 4003.54 | 0.0 |
| ILE2:HECELL† | `marker` | 4604.64 | 0.0 |
| ILE2:Q16 | `EQuad` | 4905.28 | 61.14 |
| ILE2:Q17 | `EQuad` | 4992.23 | 61.14 |
| ILE2:RPM17X/Y† | `marker` | 5064.95 | 0.0 |
| ILE2:Q18 | `EQuad` | 5143.74 | 61.14 |
| ILE2:Q19 | `EQuad` | 5233.25 | 61.14 |
| ILE2:XCB19† | `ecb` | 5313.31 | 0.0 |
| ILE2:YCB19† | `ecb` | 5365.96 | 0.0 |
| ILE2:FC19† | `fc` | 5429.94 | 0.0 |
| ILE2:Q20 | `EQuad` | 5854.46 | 61.14 |
| ILE2:YCB20† | `ecb` | 5923.29 | 0.0 |
| ILE2:XCB21 | `deflx` | 6101.27 | 55.88 |
| ILE2:B21 | `eb` | 6419.82 | 159.59 |
| ILE2A:Q2 | `EQuad` | 7172.11 | 61.14 |
| ILE2A:YCB2† | `ecb` | 7240.95 | 0.0 |
| ILE2A:RPM2† | `marker` | 7330.52 | 0.0 |
| end sequence | `marker` | 7330.52 | 0.0 |

Table 19: Sequence `ile2_db9`: The Polarizer beamline. † indicates approximate placement. All quadrupoles in this sequence use Wollnik integrals $(I_1, I_2, I_3, I_4)$ = (0.085,0.004,0.031,-0.232).

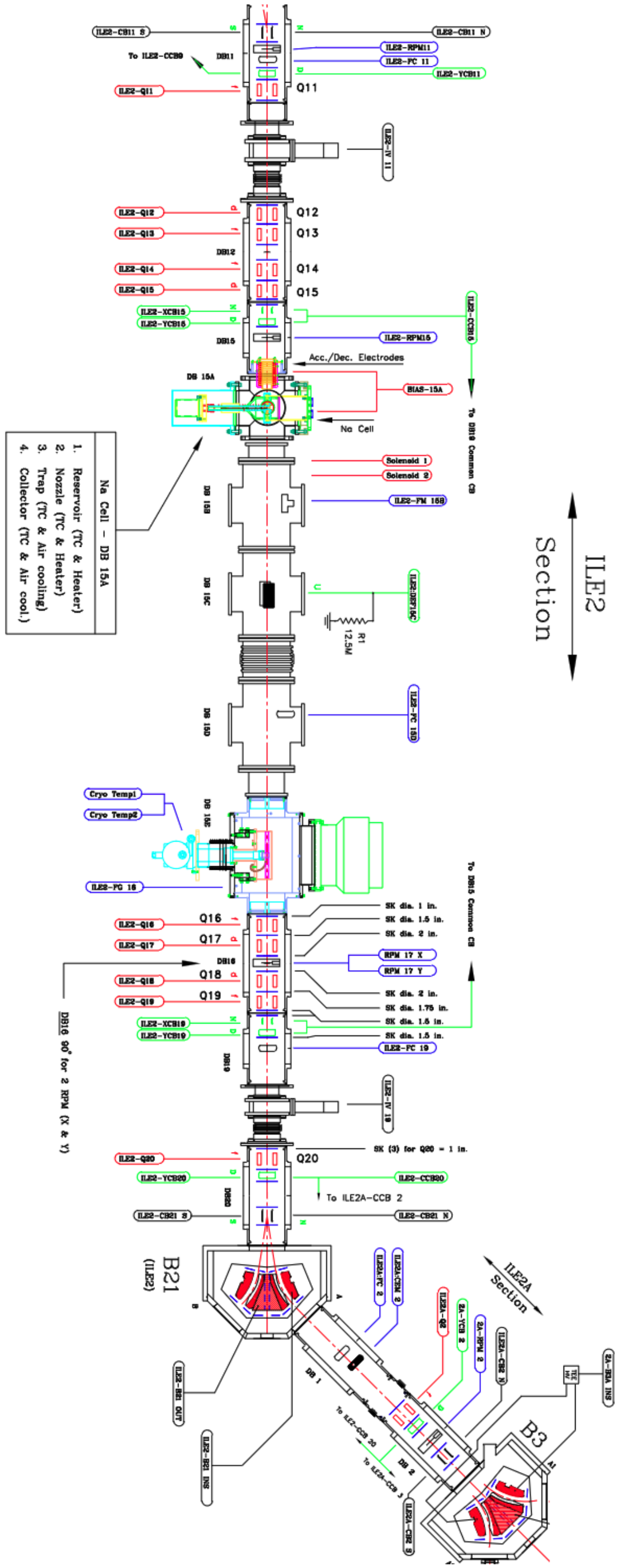


Figure 15: Sketch drawing `ISK4231D-rev11.dwg`, showing the polarizer sequence, terminating at location of ILE2A:RPM2.

# 2 Transport Tune

All reported dimensions are now in the acc-repository. The code xml2optr[3] has been used to generate TRANSOPTR files. Baartman's design tune for a 30kV, charge state 1 beam is recorded in Table 20. Beam envelopes are shown in Figure 16.

Design IMS/ILT

| Element Name | Setpoint [V] |
|---|---|
| IMS:Q11 | 1422.0 |
| IMS:Q12 | 1494.0 |
| IMS:Q15 | 1187.0 |
| IMS:Q16 | 1855.0 |
| IMS:Q17 | 0.0 |
| IMS:Q18 | 1177.0 |
| IMS:Q19 | 865.0 |
| IMS:Q20 | 1261.0 |
| IMS:Q21 | 972.0 |
| IMS:Q22 | 923.0 |
| IMS:Q24 | 1027.0 |
| IMS:Q25 | 1027.0 |
| IMS:Q29 | 495.0 |
| IMS:Q30 | 2325.0 |
| IMS:Q31 | 1075.0 |
| ILT:Q1 | 1027.0 |
| ILT:Q2 | 142.0 |
| ILT:Q3 | 612.0 |
| ILT:Q4 | 2061.0 |
| ILT:Q8 | 777.0 |
| ILT:Q9 | 1027.0 |
| ILT:Q12 | 1027.0 |
| ILT:Q15 | 1027.0 |
| ILT:Q20 | 495.0 |
| ILT:Q21 | 2325.0 |
| ILT:Q22 | 1075.0 |
| ILT:Q26 | 495.0 |

Design ILE/ILE2

| Element Name | Setpoint [V] |
|---|---|
| ILE:Q1 | 2325.0 |
| ILE:Q2 | 1075.0 |
| ILE:Q5 | 495.0 |
| ILE:Q6 | 1227.0 |
| ILE:Q7 | 689.0 |
| ILE:Q9 | 1227.0 |
| ILE:Q10 | 1027.0 |
| ILE:Q11 | 1027.0 |
| ILE:Q12 | 0.0 |
| ILE2:Q1 | 0.0 |
| ILE2:Q2 | 639.0 |
| ILE2:Q3 | 2009.0 |
| ILE2:Q4 | 1660.0 |
| ILE2:Q5 | 0.0 |
| ILE2:Q11 | 327.0 |
| ILE2:Q12 | 0.0 |
| ILE2:Q13 | 0.0 |
| ILE2:Q14 | 1192.0 |
| ILE2:Q15 | 1167.0 |
| ILE2:Q16 | 1985.0 |
| ILE2:Q17 | 1605.0 |
| ILE2:Q18 | 1605.0 |
| ILE2:Q19 | 1985.0 |
| ILE2:Q20 | 0.0 |

Table 20: Baartman's design tune, spanning exit of the ISAC mass separator (IMS:YSLIT11B), up to the end of the polarizer.

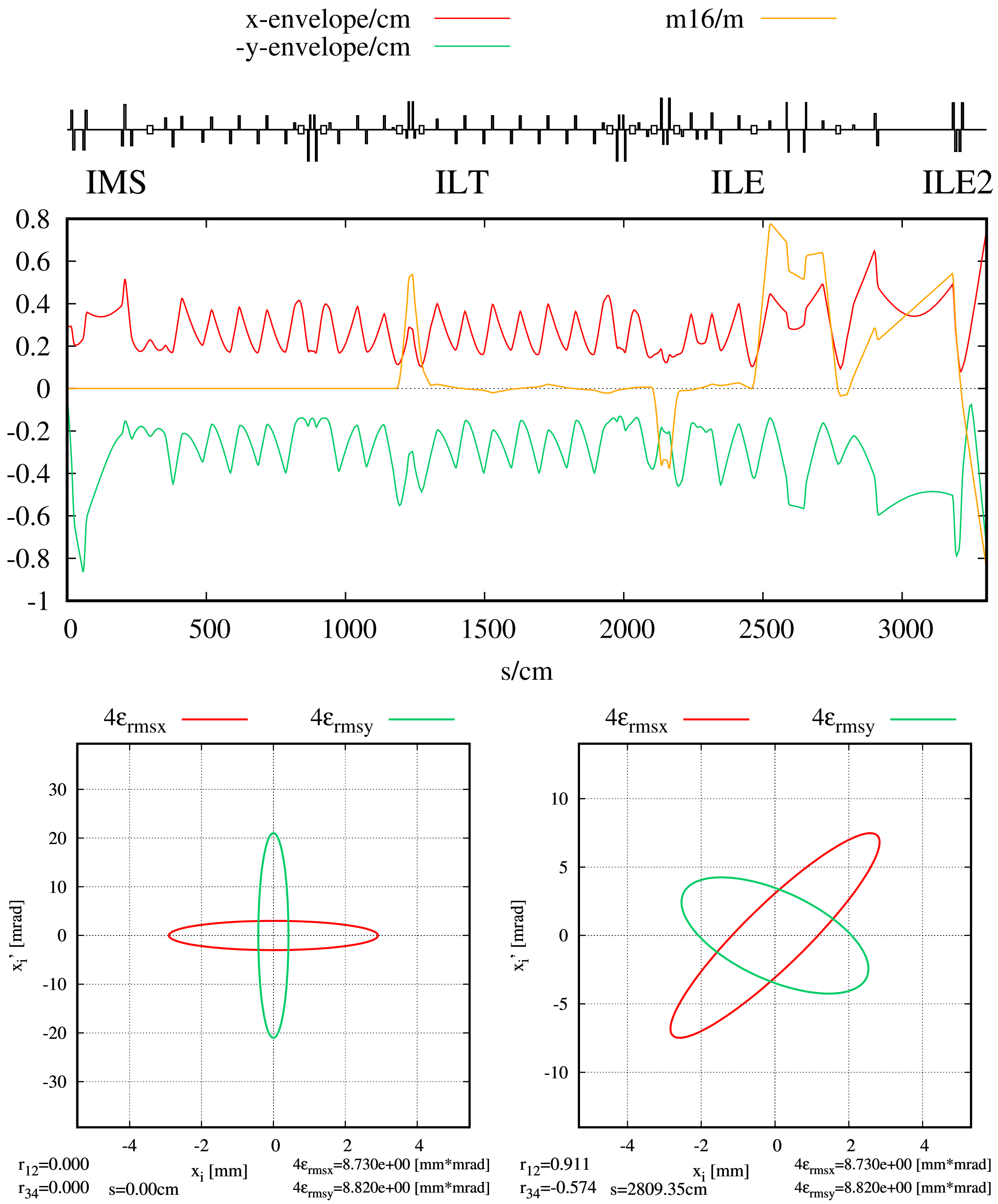


Figure 16: Design transport tune from IMS:YSLIT11B up to end of ISAC Polarizer beamline for a 30keV, charge state 1 beam. Quadrupole lattice is shown at the top of the figure in the form of the strengths. Transverse 4rms containment ellipses are shown at the bottom of the figure. The lower left plot shows distribution at YSLIT11B, while the lower right figure shows the distribution at ILE2:RPM11, at the entrance of the polarizer.

# 3 Summary

This report documented the implementation of `acc/`-repository dimensions for the IMS to polarizer radioisotope transport beamlines. Listed dimensions throughout the report have been verified against `TRANSOPTR` files maintained by the Beam Physics Dept.

# References

[1] Olivier Shelbaya. Model Coupled Accelerator Tuning (PhD thesis). Technical Report TRI-BN-23-04, TRIUMF, UVic Dept. of Physics & Astronomy, 2023. https://dspace.library.uvic.ca/handle/1828/14804.

[2] B Hartmann, M Berz, and H Wollnik. The computation of aberrations of fringing fields of magnetic multipoles and sector magnets using differential algebra. *Nuclear Instruments and Methods in Physics Research Section A: Accelerators, Spectrometers, Detectors and Associated Equipment*, 297(3):343–353, 1990.

[3] Olivier Shelbaya and Paul M. Jung. Generation of TRANSOPTR files with `xml2optr`. Technical Report TRI-BN-22-06, TRIUMF, 2022.

# Appendices

## Appendix A `fort.label` for IMS-Polarizer

```
#s [mm]     Element Centrepoint
0 YSLIT11B
151.83 IMS:Q11
228.03 IMS:Q12
591.24 IMS:Q12
669.98 IMS:Q11
1012.89 IMS:FC14
1112.89 IMS:RPM14
1974.27 IMS:Q15
2063.16 IMS:Q16
2215.53 IMS:Q17
2304.42 IMS:Q18
2642.46 IMS:RPM18
2865.67 i
2915.54 .
2965.41 IMS:B18
3015.28 .
3065.16 .
3065.16 x
3407.82 IMS:FC19
3529.19 IMS:Q19
3794.29 IMS:Q20
3934.83 IMS:LPM20
4108.39 IMS:Q21
4863.35 IMS:Q22
5052.62 IMS:RPM22
5177.4 IMS:Q23
5858.4 IMS:Q24
6048.42 IMS:RPM24
6172.55 IMS:Q25
6854.13 IMS:Q26
7168.1 IMS:Q27
7848.68 IMS:Q28
```

```
8162.65 IMS:Q29
8292.27 i
8342.15 .
8392.02 IMS:B30
8441.9 .
8491.77 .
8491.77 x
8653.08 IMS:Q30
8722.93 IMS:Q31
8798.77 IMS:RPM31
8870.76 IMS:Q32
8940.61 IMS:Q33
9104.26 i
9154.14 .
9204.01 IMS:B33
9253.89 .
9303.76 .
9303.76 x
9431.84 IMS:Q34
9553.82 IMS:LPM34
9629.66 IMS:FC34
9745.79 IMS:Q35
10426.3 IMS:Q36
10740.2 IMS:Q37
11386.9 ILT:Q1
11575.5 ILT:RPM1
11700.8 ILT:Q2
11828.7 i
11878.6 .
11928.4 ILT:VB3
11978.3 .
12028.2 .
12028.2 x
12192 ILT:Q3
12261.8 ILT:Q4
12363.3 ILT:RPM4
12409.7 ILT:Q5
12479.5 ILT:Q6
12643.4 i
12723.1 ILT:VB6
12802.8 .
```

```
12802.8 x
13037.2 defx
13045.9 ILT:RPM7
13128.2 ILT:FC7
13284.5 ILT:Q8
13965.3 ILT:Q9
14279.2 ILT:Q10
14959.6 ILT:Q11
15273.6 ILT:Q12
15954.4 ILT:Q13
16268.3 ILT:Q14
16949 ILT:Q15
17032.2 ILT:LPM15
17263 ILT:Q16
17943.4 ILT:Q17
18088.8 ILT:RPM17
18257.6 ILT:Q18
18938.1 ILT:Q19
19085.4 ILT:FC19
19252 ILT:Q20
19389.2 i
19439.1 .
19489 ILT:VB21
19538.8 .
19588.7 .
19588.7 x
19750.8 ILT:Q21
19820.6 ILT:Q22
19897 ILT:RPM22
19970.8 ILT:Q23
20040.6 ILT:Q24
20202.7 i
20252.6 .
20302.4 ILT:VB24
20352.3 .
20402.2 .
20402.2 x
20530.9 ILT:Q25
20656.3 ILT:FC25
20844.8 ILT:Q26
20977.5 i
```

```
21027.4 .
21077.3 ILE:B1
21127.2 .
21177 .
21177 x
21339.1 ILE:Q1
21409 ILE:Q2
21485.6 ILE:RPM2
21559.1 ILE:Q3
21628.9 ILE:Q4
21791 i
21840.9 .
21890.8 ILE:B4
21940.7 .
21990.5 .
21990.5 x
22098.4 ILE:Q5
22229.9 ILE:RPM5
22286.3 ILE:FC5
22412.4 ILE:Q6
22626.1 ILE:Q7
22780.9 ILE:RPM7
22940.2 ILE:Q8
23155.1 ILE:Q9
23468.9 ILE:Q10
24128.8 ILE:Q11
24442.7 ILE:Q12
24571 i
24620.8 .
24670.7 ILE2:B1
24720.6 .
24770.5 .
24770.5 x
24920.9 ILE2:Q1
25052.7 ILE2:RPM1
25106.2 ILE2:FC1
25234.9 ILE2:Q2
25842.1 ILE2:Q3
25912 ILE2:Q4
25982 ILE2:Q5
26399.6 ILE2:Q6
```

```
26469.6 ILE2:Q7
26539.4 ILE2:Q8
27146.7 ILE2:Q9
27311.8 ILE2:RPM9
27460.7 ILE2:Q10
27611.3 i
27691.1 ILE2:B10
27770.9 .
27770.9 x
28009.6 defx
28081.5 ILE2:RPM11
28132.3 ILE2:FC11
28250.4 ILE2:Q11
28782.6 ILE2:Q12
28869.5 ILE2:Q13
29021 ILE2:Q14
29110.4 ILE2:Q15
29311.3 ILE2:RPM15
30926.3 ILE2:FC15
31828 ILE2:Q16
31915 ILE2:Q17
31987.7 ILE2:RPM17X
31987.7 ILE2:RPM17Y
32066.5 ILE2:Q18
32156 ILE2:Q19
32352.7 ILE2:FC19
32777.2 ILE2:Q20
33024 defx
33262.8 i
33342.5 ILE2:B21
33422.3 .
33422.3 x
33720.6 ILE2A:FC2
34094.8 ILE2A:Q2
34253.3 ILE2A:RPM2
```